Journal of Orthopaedic Translation 45 (2024) 66–74

Contents lists available at ScienceDirect

Journal of Orthopaedic Translation

journal homepage: www.journals.elsevier.com/journal-of-orthopaedic-translation

Original Article

A novel therapy for fracture healing by increasing lymphatic drainage

Yangkang Zheng [a,b,c], Pengyu Wang [a,b,c], Li Zhao [a,b,c], Lianping Xing [d], Hao Xu [a,b,c], Ning Li [a,b,c], Yongjian Zhao [a,b,c], Qi Shi [a,b,c], Qianqian Liang [a,b,c,**], YongJun Wang [a,b,c,*]

[a] Longhua Hospital, Shanghai University of Traditional Chinese Medicine, 725 Wan-Ping South Road, 200032, Shanghai, China
[b] Spine Institute, Shanghai University of Traditional Chinese Medicine, 725 Wan-Ping South Road, 200032, Shanghai, China
[c] Key Laboratory of Theory and Therapy of Muscles and Bones, Ministry of Education (Shanghai University of Traditional Chinese Medicine), 1200 Cailun Road, 201203, Shanghai, China
[d] Department of Pathology and Laboratory Medicine and Center for Musculoskeletal Research, University of Rochester Medical Center, 601 Elmwood Avenue, Rochester, NY, 14642, USA

ARTICLE INFO

Keywords:
Fracture healing
Lymphatic drainage
Lymphatic platelet thrombosis
Podoplanin neutralizing antibody
VEGFR3 inhibitor

ABSTRACT

Background: The musculoskeletal system contains an extensive network of lymphatic vessels. Decreased lymph flow of the draining collecting lymphatics usually occurs in clinic after traumatic fractures. However, whether defects in lymphatic drainage can affect fracture healing is unclear.

Methods: To investigate the effect of lymphatic dysfunction on fracture healing, we used a selective VEGFR3 tyrosine kinase inhibitor to treat tibial fractured mice for 5 weeks versus a vehicle-treated control. To ensure successfully establishing deceased lymphatic drainage model for fractured mice, we measured lymphatic clearance by near infrared indocyanine green lymphatic imaging (NIR-ICG) and the volume of the draining popliteal lymph nodes (PLNs) by ultrasound at the whole phases of fracture healing. In addition, hindlimb edema from day 0 to day 7 post-fracture, pain sensation by Hargreaves test at day 1 post-fracture, bone histomorphometry by micro-CT and callus composition by Alcian Blue-Hematoxylin/Orange G staining at day 14 post-fracture, and bone quality by biomechanical testing at day 35 post-fracture were applied to evaluate fracture healing. To promote fracture healing via increasing lymphatic drainage, we then treated fractured mice with anti-mouse podoplanin (PDPN) neutralizing antibody or isotype IgG antibody for 1 week to observe lymphatic drainage function and assess bone repair as methods described above.

Results: Compared to vehicle-treated group, SAR-treatment group significantly decreased lymphatic clearance and the volume of draining PLNs. SAR-treatment group significantly increased soft tissue swelling, and reduced bone volume (BV)/tissue volume (TV), trabecular number (Tb.N), woven bone and biomechanical properties of fracture callus. In addition, anti-PDPN treated group significantly reduced the number of $CD41^{+}$ platelets in PLNs and increased the number of pulsatile lymphatic vessels, lymphatic clearance and the volume of PLNs. Moreover, anti-PDPN treated group significantly reduced hindlimb edema and pain sensation and increased BV/TV, trabecular number (Tb.Th), woven bone and biomechanical properties of fracture callus.

Conclusions: Inhibition of proper lymphatic drainage function delayed fracture healing. Use of a anti-PDPN neutralizing antibody reduced lymphatic platelet thrombosis (LPT), increased lymphatic drainage and improved fracture healing.

The translational potential of this article: (1) We demonstrated lymphatic drainage function is crucial for fracture healing. (2) To unblock the lymphatic drainage and prevent the risk of bleeding and mortality by blood thinner, we demonstrated PDPN neutralizing antibody is a novel and safe way forward in the treatment of bone fracture healing by eliminating LPT and increasing lymphatic drainage.

* Corresponding author.Shanghai University of Traditional Chinese Medicine, 1200 Cai Lun Road, Shanghai, 201203, China.
** Corresponding author. Spine Institute, Shanghai University of Traditional Chinese Medicine, 725 Wan-Ping South Road, Shanghai, 200032, China.
E-mail addresses: liangqianqian@shutcm.edu.cn (Q. Liang), wangyongjun@shutcm.edu.cn (Y. Wang).

https://doi.org/10.1016/j.jot.2024.02.001
Received 27 September 2023; Received in revised form 3 January 2024; Accepted 6 February 2024

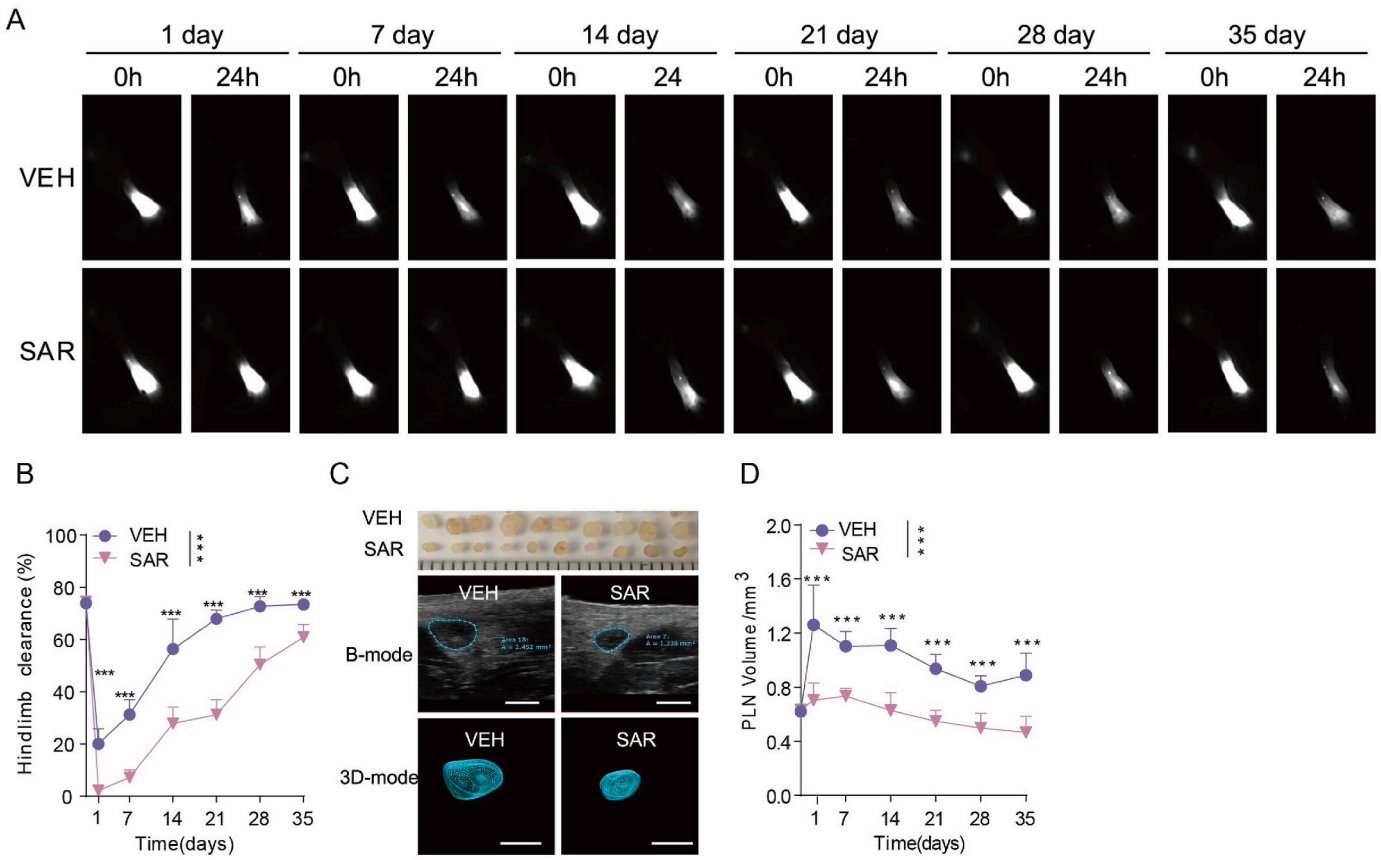

Figure 1. Blockade of VEGFR-3 signaling reduces the lymphatic drainage (A) Representative NIR-ICG images at 0 h and 24 h after ICG injection in 35 days post-fracture. (B) Quantification of lymphatic clearance at various time points (n = 10/group at each time point). (C) The gross anatomy of isolated PLNs at day 35 after fracture (top). Representative B mode and 3D mode ultrasound image of PLNs at day 35 (bottom). Scale bars, 1 mm. (D) Quantitative analysis of the PLN volume at different time points (n = 10/group at each time point). Data are means ± SD. ***P < 0.001. In B and D, analysis of variance in repeated measurement design followed the simple effect test.

1. Introduction

Lymphatic vessels (LVs) interdigitate with blood vessels and play important functions in interstitial fluid drainage, lipid absorption, and immune responses [1,2]. The musculoskeletal system, especially that in the skin, muscle and periosteum, contains an extensive network of LVs [3–5]. Previous work by Grzegorz Szczesny and colleagues on the changes of the lymphatic system in response to bone fractures [6–9], has inspired much of our work. They found that decreased lymph flow with dilatation of the draining collecting lymphatics occurs after traumatic fractures [6,7]. In addition, enlarged superficial LVs and draining lymph nodes were found in limbs with healed bone fractures, while reduced draining lymph nodes were seen in the majority of patients with non-healing fractures [8,9]. These previous findings indicate the lymphatic system is involved in fracture healing. However, the effect of proper lymphatic drainage on fracture healing is unclear.

In this study, we evaluated fracture repair with or without VEGFR3 inhibitor interventions and demonstrate that inhibiting lymphatic drainage delays fracture healing. We further identified that platelet thrombosis blocks lymphatic drainage and that treatment with a podoplanin-neutralizing antibody reduced lymphatic platelet thrombosis, improved lymphatic drainage, and enhanced fracture healing. These findings suggest that anti-PDPN neutralizing antibody is potential therapeutic target to improve fracture healing via eliminating lymphatic platelet thrombosis and increasing lymphatic drainage.

2. Material and methods

2.1. Animals

All animal experiments described in this research were approved by Shanghai University of Traditional Chinese Medicine-Animal Ethics Committee (PZSHUTCM211101023). Specific pathogen-free, 6~8-week-old male C57BL/6 mice were obtained from Shanghai Jessie Experimental Animal Co., Ltd. The mice were housed 5 per micro-isolator cage in the animal center of Shanghai model organisms on a 12-h light/dark cycle. Mice were fed with regular rodent's chow and sterilized tap water ad libitum. All mice were randomly assigned to each group and accommodate for 1 weeks before experimental procedures.

2.2. Open tibial fracture model

After one week of adaptive feeding, we performed open right tibial fracture osteotomy using a scalpel blade to transect the tibia carefully at the upper third without any injury to fibula and draining LVs behind the tibia [4], and intramedullary fixation via a 0.45 (outer gauge)×16 mm (inner gauge) intradermal needle (WEGO Holding Co., Ltd. Weihai, Shandong Province, China) [10].

2.3. VEGFR3 tyrosine kinase inhibitor administration

40 mice were equally randomly assigned to SAR group (n = 20) and VEH group (n = 20). SAR131675 (Cat. No. HY-15458, MedChemExpress, 250 mg) was dissolved in a solvent, containing 2.5 mL dimethyl

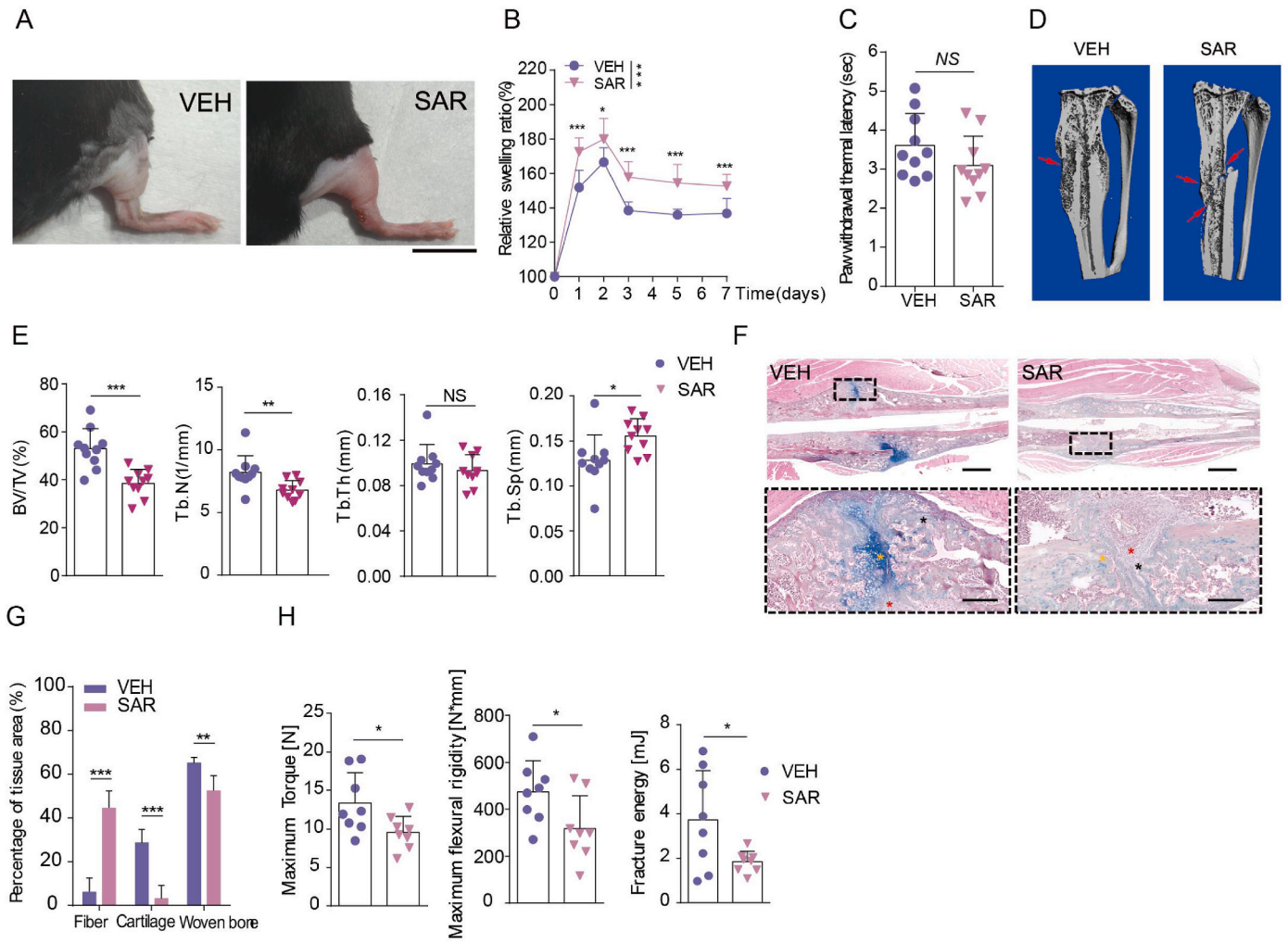

Figure 2. Blockade of VEGFR-3 signaling delays fracture healing (A) Representative photographs of hindlimb at day 2. Scale bars, 1 cm. (B) The relative swelling ratio of mouse hindlimb in 7 days after fracture (n = 10/group). (C) PWTL at day 1 (n = 10/group at each time point). (D) Representative Micro-CT images (cross-section) of tibial fracture healing at day 14 post-fracture. Red arrow indicates bone defect. (E) Quantification of BV/TV, Tb.N, Tb.Th and Tb.Sp (n = 10/group). (F) Representative histomorphological images of ABH-stained sections at day 14 post-fracture. Red asterisk indicates fiber, Orange asterisk indicates cartilage, and black asterisk woven bone. The bottom images are higher magnifications of the regions boxed in black in the corresponding image above. Scale bars, 1 mm, 200 mm. (G) Callus composition in (F) were analyzed (n = 7/group). (H) Quantification of maximum torque, maximum flexural rigidity, and fracture energy (n = 8/group). Data are means ± SD. *P < 0.05; **P < 0.01; ***P < 0.001; NS, not significant. In B, analysis of variance in repeated measurement design followed the simple effect test. In C, E, G and H, two-sided Student's t-test. (For interpretation of the references to colour in this figure legend, the reader is referred to the Web version of this article.)

sulfoxide, 15 mL polyethylene glycol, 2.5 mL Tween-80 and 30 mL double distilled water. Then the dissolved SAR131675 (50 mg/kg of body weight) was intraperitoneally injected once per day for 2 weeks or 5 weeks (5 days per week) immediately after tibial fracture established. The VEH group was given the same volume of solvent.

2.4. Near-infrared indocyanine green (NIR-ICG) lymphatic imaging

After hair removal from the hind limbs, under isoflurane anesthetization, the mice were fixed on a hot-plate universal platform with a temperature of 37 °C. The mice were subcutaneously injected with 5 μL 0.2 mg/ml ICG solution (Cat.No.17478-701-02, Akorn) into the footpads. Under an NIR laser (Changchun Laser Technology), ICG fluorescence of the afferent LVs from the injection site to the PLN were observed. (a) For lymphatic clearance, the ICG clearance was assessed by calculating the percentage clearance of footpad region of interest (ROI) at 0 h and 24 h after ICG injection. (b) For lymphatic morphology and pulse calculation, the ICG signal was recorded continuously for 300 s by an Olympus microscope (exposure times 200 ms) and synthesized as NIR real time video. Images on lymphatic clearance (a) and videos on lymphatic pulses (b) were analyzed by Image J software as previously described [11,12]. Data analysis was performed in a blinded fashion.

2.5. Ultrasound imaging

Before ultrasound image, hind limbs hair of fractured mice were moved. Under isoflurane anesthesia, the mice were fixed in a prone position on a universal hot plate platform with a constant temperature of 37 °C. The scanning parameter of mouse superficial tissue mode and 0.04 mm scanning layer thickness were applied to scan the PLNs. The images were recorded by using an MX550D ultrasonic probe fixed on the 3D Motor Assembly. The maximum cross-sectional area in B mode and the volume of PLN in 3D mode was obtained by Vevo Lab 3.2.0 software. Data analysis was performed in a blinded fashion.

2.6. Swelling measurement

At day 0–7 day post-fracture, the fractured hindlimbs of all mice

were measured soft tissue swelling by our homemade swelling meter, based on an improvement of the plethysmometer paw volume meter test for rats [13]. Briefly, we kept the right hind limb below the level of knee joint completely immersed in a container filled with liquid. The volume change in the container before and after measurement was calculated as the swelling volume of the hind limb of the mouse. Each data was measured 3 times and averaged. Swelling degree = (measurement - baseline)/baseline *100%.

2.7. Hargreaves test

On 24th hour post-fracture, thermal pain sensation in mice were measured by a dynamic plantar tester (Cat.No. 37370, Ugo Basile). A withdrawal response is termed as withdrawal latency. A longer withdrawal latency signifies a slower withdrawal response and vice versa [14]. After the mice were acclimated to the testing environment, 30% radiant heat was used to induce the withdrawal response. The paw withdrawal thermal latency (PWTL) value was recorded automatically by the instrument and was determined when the mice felt pain and raised their hind paw. Each mouse was tested five times. To obtain the average reaction time for every mouse, the lowest and the highest values were removed as outlying values and the remaining 3 values were averaged and recorded (see Figs. 2 and 5).

2.8. Micro-computed tomography analysis

The fractured tibia was harvested at day 14 post-fracture by careful dissection and removal of the intramedullary pin. The sample was fixed in 4% paraformaldehyde for 24 h, washed for 2 h, and soaked in 75% ethanol. The samples in Fig. 2 were scanned by high resolution μCT (Scanco Medical AG,vivaCT80,Switzerland), and the following parameters were used: 55 kV voltage setting, 72 μA current, 15.6 μm voxel size. The 2D-image reconstruction at an integration time of 200 ms and the 3D Calc were analyzed by the evaluation program v6.6 (Scanco Medical AG,viva CT80,Switzerland) under the threshold of 235–1000. The samples in Fig. 5 were scanned by high resolution μCT (SkyScan 1176, Bruker, Belgium), and the following parameters were used: 9 μm resolution, 0.5 mm aluminum filter, 70 kV voltage, and 142 μA current. All imaging and data were acquired by commercial software provided by the company. As previously described [15], the major parameters for callus quantity and fracture healing included bone volume/total volume (BV/TV), trabecular number (Tb.N), trabecular thickness (Tb.Th), trabecular separation (Tb.Sp).

2.9. ABH/OG staining and histomorphometric analysis

Harvested tibias scanned by micro-CT were then completely decalcified in 10% EDTA and embedded in paraffin. Paraffined specimens were cut at a thickness of 6 mm and 3 levels (each level was cut 50 μm apart). ABH/OG staining was used to evaluate tibial callus on day 14 post-fracture. Sections were stained with Alcian blue/hematoxylin (ABH) and counterstained with eosin/orange G. All stained slices were then scanned with an Olympus VS-120 whole-slide imaging system. Quantitative analysis of the callus composition were measured using SlideViewer software (version 2013.3) in a blinded manner.

2.10. Biomechanical testing

The healed tibia of the right hind leg at day 35 post-fracture was harvested and sent for three-point bending tests by a standard materials testing machine (Model 5569; Instron Corp., Norwood, MA, USA) as previously described [16]. Primary fracture sides of each tested tibia were placed at a midpoint of two supports spaced 6 mm apart. The bending load was applied at the midpoint at a constant displacement rate of 1 mm/min until the sample fractured. Maximum torque, maximum flexural rigidity and fracture energy were calculated by a custom program (MATLAB; MathWorks Inc., Natick, MA, USA). All samples were blinded throughout preparation and testing.

2.11. Immunofluorescence staining of fracture sides

Immunofluorescence staining of tibial callus on 14d post fracture was used to quantitative analysis of blood vessels and lymphatic vessels. Heat-induced antigen retrieval for dewaxed paraffin sections followed the manufacture's instruction (Cat. No. P0081, Beyotime). Then, the sections were blocked by 0.3% PBST with 5% bovine serum albumin for 1 h at room temperature, then incubated with primary antibodies overnight at 4 °C. After washing with PBS, secondary antibodies were incubated for 2 h at room temperature. Finally, the sections were mounted with 4,6-diamidino-2-phenylindole (Cat.No. H-1200, Vectorlabs). The primary antibodies included syrian hamster monoclonal anti-podoplanin antibody (Cat.No. ab11936, Abcam Inc., Cambridge, MA, 1:1000) and rabbit monoclonal anti-CD31 antibody (Cat.No. ab182981, Abcam Inc., 1:1000). The corresponding secondary antibodies were used as follows: Alexa Fluor 488 goat anti-hamster antibody (Cat. No. A-21110, Invitrogen, 1:200), Alexa Fluor 555 goat anti-rat antibody (Cat. No. 4417S, Cell Signaling Technology, 1:1000). Three randomized images per paraffin section were acquired by using an Olympus VS120 microscope under a 10 × objective.

A continuous endothelial monolayer with CD31 positive and Podoplanin negative markers was regarded as blood vessels, while with Podoplanin positive and CD31 negative markers was regarded as lymphatic vessels [17,18]. The number of blood vessels and lymphatic vessels per magnification (×10) image in fracture sides was calculated by manual counting. The mean value of three magnification (×10) images of each paraffin section was calculated as one sample data. Data analysis was performed in a blinded fashion with regard to group allocations.

2.12. Transmission electron microscopy

The draining popliteal lymph nodes of fractured mice on day 4 post-fracture were harvested and fixed with 2.5% glutaraldehyde in 0.1 M PBS, pH 7.4, for 24 h. Then the specimens were fixed in 1% buffered osmium tetroxide for 2 h at 4 °C, dehydrated through a graded series of ethanol, infiltrated/embedded into acetone/resin and polymerized at 60 °C for 3 days. The specimens were sliced with one-micron thick. 70 nm thin sections were mounted onto 200 mesh carbon-coated nickel grids and stained with lead citrate for ultrastructural examination. At last, the grids were examined and photographed using a FEI Tecnai G2 Spirit transmission electron microscope.

2.13. Immunofluorescence staining of PLNs

After harvest, the lymph nodes were photographed. For tissue processing, PLNs were fixed in 4% paraformaldehyde, dehydrated in a gradient sucrose solution, embedded in OCT and stored at −80 °C. A cryostat (Leica, CM3050S) was then used to cut 7-μm-thick frozen sections. For immunofluorescence staining, sections were blocked by 0.3% PBST with 5% bovine serum albumin for 1 h at room temperature, then incubated with primary antibodies overnight at 4 °C. After washing with PBS, secondary antibodies were incubated for 2 h at room temperature. Finally, the sections were mounted with 4,6-diamidino-2-phenylindole (Cat.No. H-1200, Vectorlabs). The primary antibodies included syrian hamster monoclonal anti-podoplanin antibody (Cat.No. ab11936, Abcam Inc., Cambridge, MA, 1:1000) and rabbit monoclonal anti-CD41 antibody (Cat.No. ab134131, Abcam Inc., 1:1000). The corresponding secondary antibodies were used as follows: Alexa Fluor 488 goat anti-hamster antibody (Cat. No. A-21110, Invitrogen, 1:200), Alexa Fluor 555 goat anti-rat antibody (Cat.No. 4417S, Cell Signaling Technology, 1:1000). Images were acquired by using an Olympus VS120 microscope under a 20 × objective.

The number of LPTs per magnification (×20) image in PLNs was by

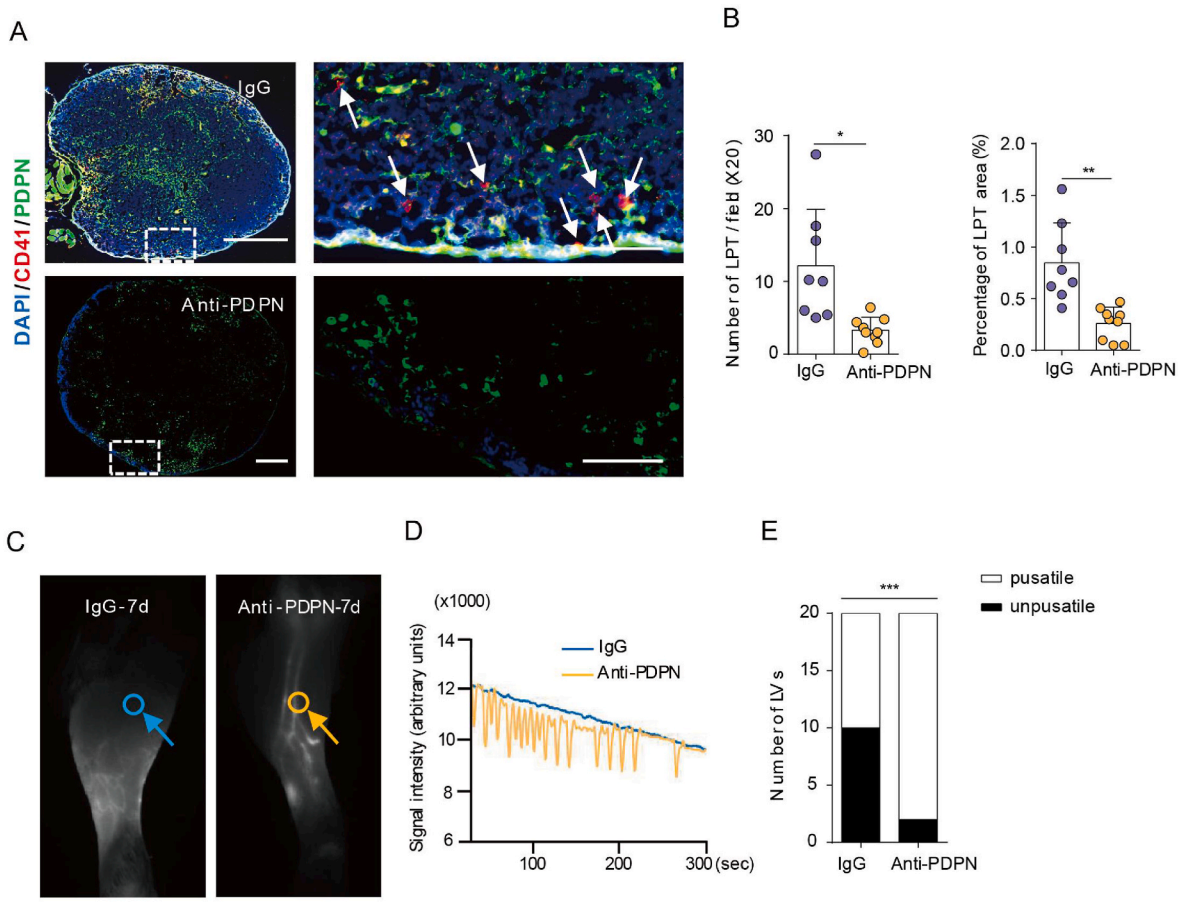

Figure 3. Anti-PDPN prevents lymphatic platelet thrombosis and unblocks lymphatic vessels (A) Representative immunofluorescence staining on PLNs using anti-CD41 antibody to label platelet (red) and anti-podoplanin antibody for LVs (green). The right images are higher magnifications of the regions boxed in white in the corresponding image above (n = 10/group). Scale bars, 200 mm, 50 mm. (B) Quantitative analysis of LPT number per field (x20) and LPT coverage area percentage (n = 8 in IgG group and n = 9 in anti-PDPN group). (C–D) Representative NIR-ICG images showing draining LVs' morphology and ROIs where the lymphatic pulses were measured (Blue circle indicates ROI at LVs from IgG group. Orange circle indicates ROI at LVs from anti-PDPN group). The interrupted ICG signal in the fractured hindlimb at day 7, marked by a blue circle, is defined as a blocked LV. (E) Number of LVs with or without lymphatic pulse at day 7 (n = 20/group). Data are means ± SD. *P < 0.05; **P < 0.01; ***P < 0.001. In B, two-sided Student's t-test. In E, Fisher's Exact Test. (For interpretation of the references to colour in this figure legend, the reader is referred to the Web version of this article.)

manual counting, both aggregated and scattered CD41+ platelets included. The coverage area ratio and the diameter of LPT was measured by ImageJ software. The mean value of five magnification (x20) images of each PLN was calculated as one sample data. Data analysis was performed in a blinded fashion with regard to group allocations.

2.14. Podoplanin neutralizing antibody treatment

60 mice were equally randomly assigned to SAR group (n = 30) and VEH group (n = 30). Anti-mouse Podoplanin antibody (Cat. No. BE0236, BioXcell) was dissolved in PBS and intramuscularly injected near the right popliteal lymph node at a dose of 25 μg per mouse at a time. Anti-mouse Podoplanin antibody was injected for 4times successively (once every two days) and start at 2 days before the fracture osteotomy. And the antibody was control mice were injected with the same dose of immunoglobulin G (IgG), polyclonal Syrian hamster IgG (Cat. No. BP0087, BioXcell).

2.15. Statistical analysis

SPSS 20.0 software was used for statistical analyses. For measurement data, data are expressed as the means ± standard deviation (SD). All continuous numerical variables approximately accord with normal distribution test by kurtosis and skewness method. Comparisons between 2 different groups were analyzed using two-sided Student's *t*-test. Paired *t*-test was used for the same group before and after comparison. A repeated measurements study was analyzed by using repeated measurement analysis of variance. *P < 0.05, **P < 0.01, and ***P < 0.001 means statistically significant difference.

3. Results

It is well known that the VEGFC/VEGFR3 signaling pathway is critical for lymphangiogenesis and LV function [19]. To investigate the effect of lymphatic dysfunction on fracture healing, we used a selective VEGFR3 tyrosine kinase inhibitor, SAR131675 (SAR), to treat mice with fracture versus a vehicle (VEH) -treated control. After fracture, mice were intraperitoneally injected with SAR131675 or solvent once a day for 14 or 35 days (5 days per week). To ensure successfully establishing deceased lymphatic drainage model on fractured mice, we firstly measure lymphatic clearance by near infrared indocyanine green lymphatic imaging (NIR-ICG) and the volume of the popliteal lymph nodes (PLNs) by ultrasound. We found that both two groups sharply decreased lymphatic clearance at day 1 post-fracture (Fig. 1A–B). Lymphatic clearance and the volumes of PLNs were significantly lower in the SAR-treated group compared to the vehicle-treated group at every time point during the entire fracture healing process (Fig. 1C–D). These results indicate that VEGFR3 tyrosine kinase inhibitor decreased

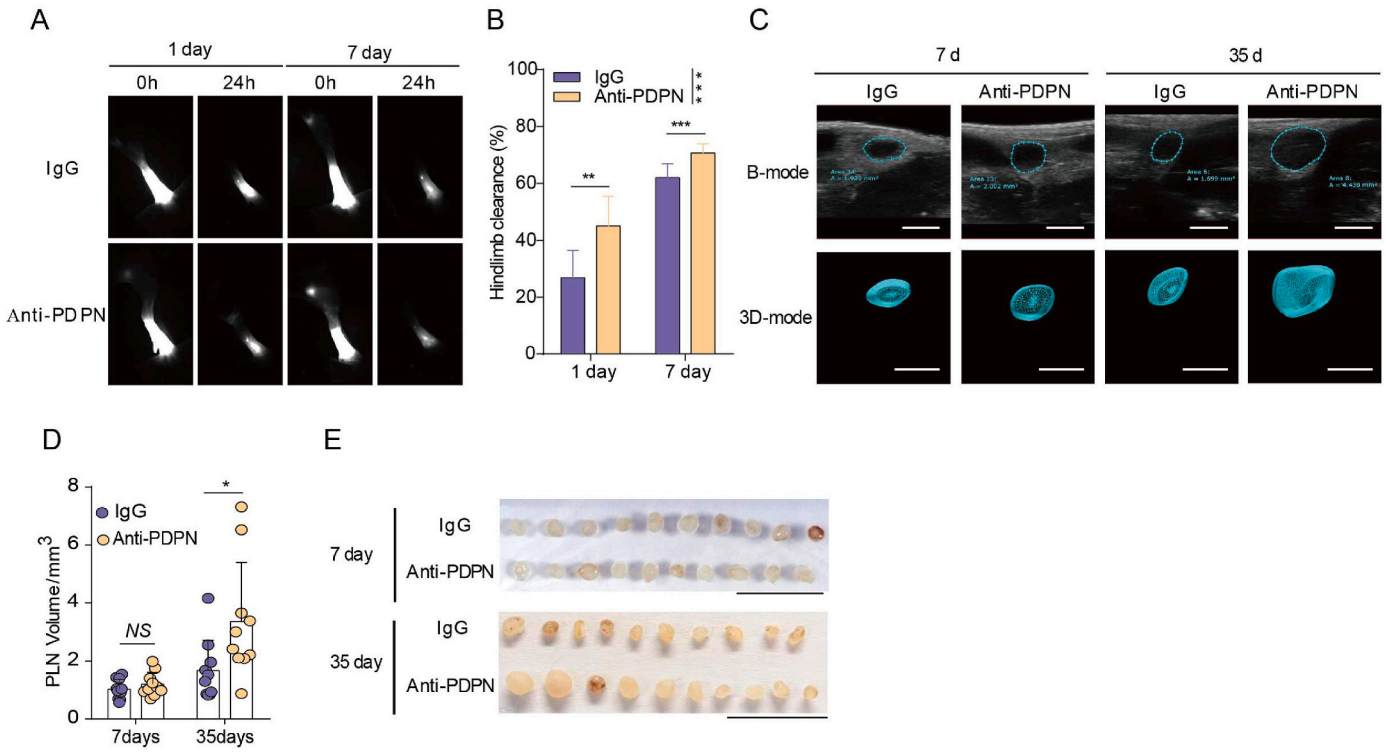

Figure 4. Anti-PDPN promotes lymphatic drainage function (A) Representative NIR-ICG images at 0 h and 24 h after ICG injection at day 1 and day 2 post-fracture. (B) Quantification of lymphatic clearance at day 1 and day 7 post-fracture (n = 10/group at each time point). (C) Representative B mode and 3D mode ultrasound image of PLNs at day 7 and day 35 post-fracture. Scale bars, 1 mm. (D) Quantitative analysis of the PLN volume at day 7 and day 35 post-fracture (n = 10/group at each time point). (E) The gross anatomy of isolated PLNs at day 7 and day 35 post-fracture. Data are means ± SD. *P < 0.05; **P < 0.01; ***P < 0.001. In B and D, two-sided Student's t-test.

lymphatic drainage for the whole phase of fractured mice.

To determine the lymphatic dysfunction on fracture healing, we examined hindlimb edema from day 0 to day 7 post-fracture, pain sensation in the fractured hindlimb by paw withdrawn threshold lentancy (PWTL) at day 1 post-fracture, bone volume by micro-CT and callus composition by Alcian Blue-Hematoxylin/Orange G (ABH/OG) -staining at day 14 post-fracture, and bone quality by biomechanical testing at day 35 post-fracture. SAR-treatment significantly increased soft tissue swelling from day 1 to day 7 after fracture initiation (Fig. 2A–B). SAR-treated group has no significant difference of PWTL with VEH-treated group probably because both groups reached the maximum threshold of pain sensation (Fig. 2C). Micro-CT reconstruction imaging showed that SAR treatment significantly reduced bone volume (BV)/tissue volume (TV), trabecular number (Tb.N), and significantly increased trabecular separation (Tb.Sp) of the fracture callus at day 14, compared to the VEH-treated group (Fig. 2D–E). ABH-staining and histomorphological analysis indicated that SAR-group had significantly increased fiber and cartilage and reduced woven bone compared to the VEH-treated group (Fig. 2F–G). Biomechanical testing showed that SAR treatment significantly decreased maximum torque, maximum flexural rigidity, and fracture energy, compared to the VEH-treated group (Fig. 2H). VEGFR3 signaling is also essential for blood vascular development and angiogenesis [20,21]. To further assess the effect of SAR13675 on lymphatic and blood vessels, we conducted quantitative analysis of blood vessels (marked with CD31) and lymphatic vessels (marked with PDPN) by immunostaining of fracture sides on 14 days post-fracture (Supplementary Fig. 1). We found that the number of lymphatic vessels was significantly decreased in SAR group while the number of blood vessels showed no obvious difference between VEH and SAR group. This suggests that SAR13675 blocked lymphangiogenesis instead of angiogenesis during fractured healing. Collectively, these results demonstrate that further exacerbation of lymphatic drainage by VEGFR3 inhibition delays fracture healing.

Since sufficient lymphatic drainage is crucial for bone repair, we attempted to study the underlying mechanism of lymphatic drainage insufficiency at the first 14 days post-fracture. We identified that activated platelet aggregates within lymphatic vessels, leading to block lymphatic drainage at the early phase of fracture healing [22]. To eliminate lymphatic platelet thrombosis (LPT), we further administered one tenth of the clinical dosage of Clopidogrel and observed that Clopidogrel improved fracture healing via unblocking lymphatic drainage [22].

Considering increasing the risk of bleeding and mortality with antithrombotic therapy during perioperative period, it's mandatory to explore a novel and safer approach to inhibiting LPT and unblocking lymphatic vessels. Large numbers of platelets are transported to draining lymphatic vessels and lymph nodes upon bone fracture and vessel rupture. The ultra-microstructure of PLNs in fractured mice showed that unactivated platelet crossed the lymphatic endothelial cell wall (Supplemental Fig. 2A). Degranulated and aggregated platelets adhered to the lymphatic endothelial cell (LEC) wall (Supplemental Fig. 2B). We inferred LECs might interact with platelet.

Podoplanin (PDPN), a well-recognized specific marker of LECs, can bind to platelet surface C-type lectin-like receptor 2 (CLEC-2) to activate platelets and form a thrombosis [23–25]. Inhibition of podoplanin, deceases deep vein thrombosis via blocking via CLEC2-PDPN signaling pathway [26,27]. Therefore, we hypothesized that anti-PDPN therapy would prevent LPT, thus improving lymphatic drainage and fracture healing. In addition, PDPN is secreted by naïve osteocytes and is an early marker for osteocyte differentiation [28,29]. *PDPN* mRNA is upregulated at day 3 post fracture and maintained with high levels of expression throughout all of the early stages of bone repair. However, the function of PDPN expressed in osteocyte in fracture healing remains unclear [28]. To test our hypothesis, we applied local injection of PLNs

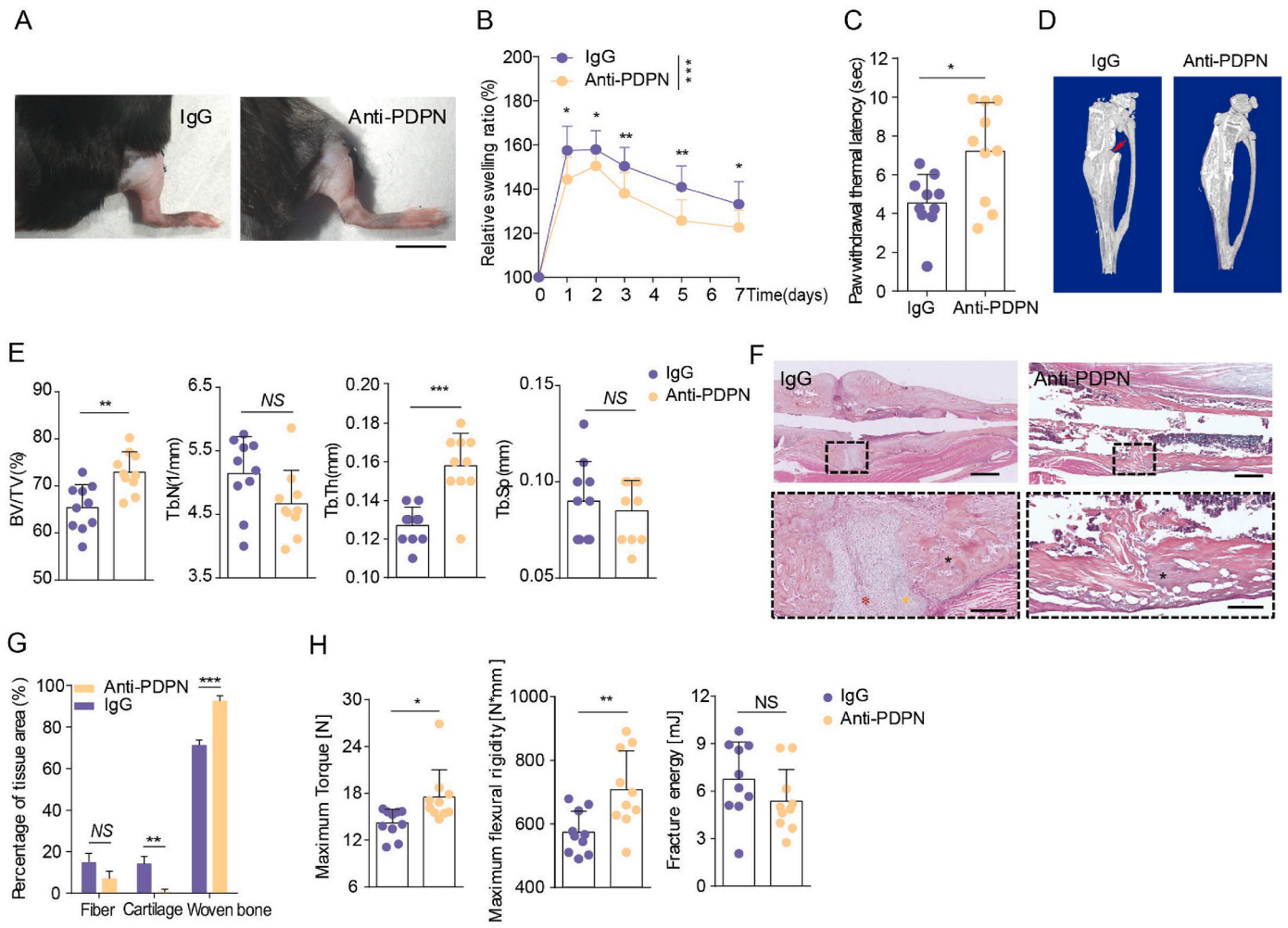

Figure 5. Anti-PDPN improves fracture healing (A) Representative photographs of hindlimb at day 2. Scale bars, 1 cm. (**B**) The relative swelling ratio of mouse hindlimb in 7 days after fracture (n = 10/group at each time point). (**C**) PWTL at day 1 (n = 10/group). (**D**) Representative Micro-CT images (cross-section) of tibial fracture healing at day 14 post-fracture. Red arrow indicates bone defect. (**E**) Quantification of BV/TV, Tb.N, Tb.Th and Tb.Sp (n = 10/group). (**F**) Representative histomorphological images of ABH-stained sections at day 14 post-fracture. Red asterisk indicates fiber, Orange asterisk indicates cartilage, and black asterisk woven bone. The bottom images are higher magnifications of the regions boxed in black in the corresponding image above. Scale bars, 1 mm, 200 mm. (**G**) Callus composition in (**F**) were analyzed (n = 6 in IgG group and n = 7 in anti-PDPN group). (**H**) Quantification of maximum torque, maximum flexural rigidity, and fracture energy (n = 10/group). Data are means ± SD. $^{*}P < 0.05$; $^{**}P < 0.01$; $^{***}P < 0.001$; *NS*, not significant. In **B**, analysis of variance in repeated measurement design followed the simple effect test. In **C**, **E**, **G** and **H**, two-sided Student's *t*-test. (For interpretation of the references to colour in this figure legend, the reader is referred to the Web version of this article.)

with anti-mouse podoplanin neutralizing antibody, starting 2 days before fracture initiation and discontinuing treatment at day 7 post-fracture, in our mouse model. On day 7 post-fracture, we measured lymphatic morphology and pulse by NIR-ICG. Then we harvested PLNs of fractured hindlimb to evaluate the number and coverage area of LPT by Immunofluorescence staining of PLNs. Compared with IgG control treatment, we found that anti-podoplanin therapy significantly reduced the number of $CD41^{+}$ platelets in PLNs (Fig. 3A–B) and increased the number of pulsatile LVs at day 7 post-fracture (Fig. 3C–E and supplementary video 1-2). These results demonstrate that anti-PDPN therapy inhibits LPT and unblocks lymphatic vessels.

Supplementary data related to this article can be found online at https://doi.org/10.1016/j.jot.2024.02.001

To evaluate the effect of anti-PDPN therapy on lymphatic drainage function, we measured lymphatic clearance by near infrared indocyanine green lymphatic imaging (NIR-ICG) and the volume of the popliteal lymph nodes (PLNs) by ultrasound on day 7 and 35 post-fracture. Compared to IgG group, anti-PDPN group significantly increased lymphatic clearance at day 7 and day 35 post-fracture by (NIR-ICG) (Fig. 4A–B), and volume of draining (PLNs) at day 35 post-fracture by ultrasound (Fig. 4C–E). These results indicate that anti-PDPN therapy promotes lymphatic drainage function.

To determine the effect of anti-PDPN therapy for fracture healing, we examined hindlimb edema from day 0 to day 7 post-fracture, pain sensation in the fractured hindlimb by paw withdrawn threshold lentancy (PWTL) at day 1 post-fracture, bone volume by micro-CT and callus composition by Alcian Blue-Hematoxylin/Orange G (ABH/OG) -staining at day 14 post-fracture, and bone quality by biomechanical testing at day 35 post-fracture. Compared to IgG controls, anti-PDPN group significantly reduced hindlimb edema post-fracture (Fig. 5A–B) and pain sensation (Fig. 5C). In addition, anti-PDPN group significantly increased BV/TV and Tb.Th (Fig. 5D–E) and woven bone (Fig. 5F–G) of fracture callus at day 14 post-fracture. Biomechanical testing indicates that anti-PDPN group significantly increased maximum torque and maximum flexural rigidity at day 35 post-fracture (Fig. 5H). These results show that anti-podoplanin therapy improves fracture healing.

4. Discussion

In this study, we firstly demonstrate that inhibiting lymphatic

drainage delays fracture healing. Then we applied PDPN neutralizing antibody to improve fracture healing. These results suggests that PDPN neutralizing antibody is potential therapeutic target to improve fracture healing via eliminating lymphatic platelet thrombosis and unblocking lymphatic drainage.

Recently, Biswas et al. utilized light-sheet microscopy technology and identified lymphatic vessel network within bone marrow cavity and bones [5]. They also demonstrate that lymphangiocrine function of secreting CXCL12 to relieved chemoradiotherapy induced bone injury [5]. This brilliant and novel work supports anatomical and functional relationship between LVs and bone. However, the effect of lymphatic drainage function on bone fracture remains unknown. Our research is a complementary work on lymphatic associated bone repair from the view of lymphatic drainage function rather than lymphangiocrine function.

Clopidogrel, a $P2Y_{12}$ antagonist, interferes with platelet activation mediated by ADP, inhibits platelet aggregation and is widely prescribed to inhibit platelet thrombosis in the clinic [30]. However, use of Clopidogrel in trauma patients or perioperative management for thromboprophylaxis increases high risk of bleeding and mortality [31–33]. In addition, large dosage of Clopidogrel for long term inhibits bone cell formation, differentiation, and activity in vitro and decreases trabecular bone in vivo [34]. To prevent the side effects of anti-coagulate agents, we advocate PDPN neutralizing antibody as a potential and safe agent for bone repair without increasing the risk of bleeding and mortality.

Post traumatic edema delays the time for surgical intervention, increases the risk of wound infection and even progresses to osteofascial compartment syndrome in some severe cases [35]. In addition, prompt treatment of pain, widely-regarded as the fifth vital sign, is beneficial for reducing suffering, readmissions and emergency department visits after hospital discharge [36]. Although many studies have reported on how to eliminate chronic post-traumatic lymphedema [37–39], the effect of lymphatic drainage on acute post-traumatic hematoma and pain is not clear. With the treatment of anti-PDPN neutralizing antibody, we determined that improving lymphatic drainage reduces acute post-traumatic edema and pain, suggesting that defects in lymphatic drainage plays a key role in the early complications of traumatic fracture.

Our study has several limitations. (1) An extensive network of LVs travels along the skin, muscle and periosteum [3–5], those supply an anatomical and physiological condition of regulating various bone repair associated cells. We will select multiple time points post-fracture, to comprehensively asses bone healing and reveal the bone repair mechanism regulated by lymphatic drainage function. (2) In Fig. 5E, as a limitation of local injection with relative high concentration of antibodies and treating control group with polyclonal IgG antibody, significant deviation within groups and little difference were shown between IgG and anti-PDPN groups probably cause by the deviation of administrative volume or/and acute inflammatory and immune response. (3) From the translational point of view, we will design a clinical research study on traumatic fracture with anti-PDPN therapy to further verify its clinical efficacy.

Author contributions

YKZ, LPX, QQL,YJW conceived and designed the study; YKZ, PYW, LZ, HX, NL, and YJZ performed the experiments and analyzed the data; YKZ drafted the manuscript; YKZ, LPX, QS, QQL and YJW revised the manuscript. All authors have approved the final version of the manuscript and have agreed to be accountable for all aspects of the work.

Data availability

The data that support the findings of this study are available from the authors upon reasonable request.

Funding

This work was sponsored by research grants from National Natural Science Foundation (81822050 and 81920108032 to QQL, 82174407 to YJZ), State Administration of Traditional Chinese Medicine Young Qi Huang Scholar, Leading medical talents in Shanghai (2019LJ02 to QQL), Dawn plan of Shanghai Municipal Education Commission (19SG39 to QQL), National Institute of Health, USA (R01 AG059775 to LPX).

Declaration of competing interest

All authors ensure no conflict of interest.

Acknowledgement

We thank to Professor Junling Liu from Shanghai Jiao Tong University School of Medicine for guidance of platelet biology. We thank to Xiong Lu, Lin Yuan, Yi Jiang from Science and Technology Experiment Center in Shanghai University of Traditional Chinese Medicine for ultrastructural identification of PLNs and LPT.

Appendix A. Supplementary data

Supplementary data to this article can be found online at https://doi.org/10.1016/j.jot.2024.02.001.

References

[1] Wiig H, Swartz MA. Interstitial fluid and lymph formation and transport: physiological regulation and roles in inflammation and cancer. Physiol Rev 2012 Jul;92(3):1005–60.
[2] Petrova TV, Koh GY. Biological functions of lymphatic vessels. Science 2020 Jul 10; 369(6500):eaax4063.
[3] van Zanten MC, Mistry RM, Suami H, Campbell-Lloyd A, Finkemeyer JP, Piller NB, et al. The lymphatic response to injury with soft-tissue reconstruction in high-energy open tibial fractures of the lower extremity. Plast Reconstr Surg 2017 Feb; 139(2):483–91.
[4] Nakajima Y, Asano K, Mukai K, Urai T, Okuwa M, Sugama J, et al. Near-infrared fluorescence imaging directly visualizes lymphatic drainage pathways and connections between superficial and deep lymphatic systems in the mouse hindlimb. Sci Rep 2018 May 4;8(1):7078.
[5] Biswas L, Chen J, De Angelis J, Singh A, Owen-Woods C, Ding Z, et al. Lymphatic vessels in bone support regeneration after injury. Cell 2023 Jan 19;186(2): 382–397.e24.
[6] Szczesny G, Olszewski WL. The pathomechanism of posttraumatic edema of lower limbs: I. The effect of extravasated blood, bone marrow cells, and bacterial colonization on tissues, lymphatics, and lymph nodes. J Trauma 2002 Feb;52(2): 315–22.
[7] Szczesny G, Olszewski WL. The pathomechanism of posttraumatic edema of the lower limbs: II–Changes in the lymphatic system. J Trauma 2003 Aug;55(2):350–4.
[8] Szczesny G, Olszewski WL, Gorecki A. Lymphoscintigraphic monitoring of the lower limb lymphatic system response to bone fracture and healing. Lymphatic Res Biol 2005;3(3):137–45.
[9] Szczesny G, Olszewski WL, Gewartowska M, Zaleska M, Górecki A. The healing of tibial fracture and response of the local lymphatic system. J Trauma 2007 Oct;63 (4):849–54.
[10] Liu J, Zhang J, Lin X, Boyce BF, Zhang H, Xing L. Age-associated callus senescent cells produce TGF-β1 that inhibits fracture healing in aged mice. J Clin Invest 2022 Apr 15;132(8):e148073.
[11] Liang Q, Zhang L, Xu H, Li J, Chen Y, Schwarz EM, et al. Lymphatic muscle cells contribute to dysfunction of the synovial lymphatic system in inflammatory arthritis in mice. Arthritis Res Ther 2021 Feb 19;23(1):58.
[12] Zhou Q, Wood R, Schwarz EM, Wang YJ, Xing L. Near-infrared lymphatic imaging demonstrates the dynamics of lymph flow and lymphangiogenesis during the acute versus chronic phases of arthritis in mice. Arthritis Rheum 2010 Jul;62(7):1881–9.
[13] Shejawal N, Menon S, Shailajan S. A simple, sensitive and accurate method for rat paw volume measurement and its expediency in preclinical animal studies. Hum Exp Toxicol 2014 Feb;33(2):123–9.
[14] Cheah M, Fawcett JW, Andrews MR. Assessment of thermal pain sensation in rats and mice using the Hargreaves test. Bio Protoc 2017 Aug 20;7(16):e2506.
[15] Jin ZX, Liao XY, Da WW, Zhao YJ, Li XF, Tang DZ. Osthole enhances the bone mass of senile osteoporosis and stimulates the expression of osteoprotegerin by activating β-catenin signaling. Stem Cell Res Ther 2021 Feb 27;12(1):154.
[16] Shi C, Hu B, Guo L, Cao P, Tian Y, Ma J, et al. Strontium ranelate reduces the fracture incidence in a growing mouse model of osteogenesis imperfecta. J Bone Miner Res 2016 May;31(5):1003–14.

[17] Baluk P, McDonald DM. Markers for microscopic imaging of lymphangiogenesis and angiogenesis. Ann N Y Acad Sci 2008;1131:1–12.
[18] Wong LL, Lee NG, Amarnani D, Choi CJ, Bielenberg DR, Freitag SK, et al. Orbital angiogenesis and lymphangiogenesis in thyroid eye disease: an analysis of vascular growth factors with clinical correlation. Ophthalmology 2016 Sep;123(9):2028–36.
[19] Pytowski B, Goldman J, Persaud K, Wu Y, Witte L, Hicklin DJ, et al. Complete and specific inhibition of adult lymphatic regeneration by a novel VEGFR-3 neutralizing antibody. J Natl Cancer Inst 2005 Jan 5;97(1):14–21.
[20] Laakkonen P, Waltari M, Holopainen T, Takahashi T, Pytowski B, Steiner P, et al. Vascular endothelial growth factor receptor 3 is involved in tumor angiogenesis and growth. Cancer Res 2007 Jan 15;67(2):593–9.
[21] Dumont DJ, Jussila L, Taipale J, Lymboussaki A, Mustonen T, Pajusola K, et al. Cardiovascular failure in mouse embryos deficient in VEGF receptor-3. Science 1998 Oct 30;282(5390):946–9.
[22] Wang YJ, Zheng Y, Cong L, Wang P, Zhao L, Xing L, et al. Lymphatic platelet thrombosis limits bone repair by precluding lymphatic transporting DAMPs. Res Sq [Preprint] 2023. Nov 14:rs.3.rs-3474507.
[23] Bertozzi CC, Schmaier AA, Mericko P, Hess PR, Zou Z, Chen M, et al. Platelets regulate lymphatic vascular development through CLEC-2-SLP-76 signaling. Blood 2010 Jul 29;116(4):661–70.
[24] Herzog BH, Fu J, Wilson SJ, Hess PR, Sen A, McDaniel JM, et al. Podoplanin maintains high endothelial venule integrity by interacting with platelet CLEC-2. Nature 2013 Oct 3;502(7469):105–9.
[25] Suzuki-Inoue K. Platelets and cancer-associated thrombosis: focusing on the platelet activation receptor CLEC-2 and podoplanin. Blood 2019 Nov 28;134(22):1912–8.
[26] Payne H, Ponomaryov T, Watson SP, Brill A. Mice with a deficiency in CLEC-2 are protected against deep vein thrombosis. Blood 2017 Apr 6;129(14):2013–20.
[27] Takemoto A, Miyata K, Fujita N. Platelet-activating factor podoplanin: from discovery to drug development. Cancer Metastasis Rev 2017 Jun;36(2):225–34.
[28] Hadjiargyrou M, Rightmire EP, Ando T, Lombardo FT. The E11osteoblastic lineage marker is differentially expressed during fracture healing. Bone 2001;29:149–54.
[29] Zhang K, Barragan-Adjemian C, Ye L, Kotha S, Dallas M, Lu Y, et al. E11/gp38 selective expression in osteocytes: regulation by mechanical strain and role in dendrite elongation. Mol Cell Biol 2006 Jun;26(12):4539–52.
[30] Jackson SP. Arterial thrombosis–insidious, unpredictable and deadly. Nat Med 2011 Nov 7;17(11):1423–36.
[31] British National Formulary 62. British Medical Journal Publishing Group Limited/Royal Pharmaceutical Society Publishing; 2011..
[32] Douketis JD, Berger PB, Dunn AS, Jaffer AK, Spyropoulos AC, Becker RC, et al. The perioperative management of antithrombotic therapy: American college of chest physicians evidence-based clinical practice guidelines (8th edition). Chest 2008;133. 299S–29S.
[33] Eeagle KA, Guyton RA, Davidoff R, Edwards FH, Ewy GA, Gardner TJ, et al. ACC/AHA 2004 guideline update for coronary artery bypass graft surgery: a report of the American College of Cardiology/American Heart Association Task Force on Practice Guidelines. Circulation 2004;110:e340–437.
[34] Syberg S, Brandao-Burch A, Patel JJ, Hajjawi M, Arnett TR, Schwarz P, et al. Clopidogrel (Plavix), a P2Y12 receptor antagonist, inhibits bone cell function in vitro and decreases trabecular bone in vivo. J Bone Miner Res 2012 Nov;27(11):2373–86.
[35] Rohner-Spengler M, Frotzler A, Honigmann P, Babst R. Effective treatment of posttraumatic and postoperative edema in patients with ankle and hindfoot fractures: a randomized controlled trial comparing multilayer compression therapy and intermittent impulse compression with the standard treatment with ice. J Bone Joint Surg Am 2014 Aug 6;96(15):1263–71.
[36] Pozza DH, Azevedo LF, Castro Lopes JM. Pain as the fifth vital sign-A comparison between public and private healthcare systems. PLoS One 2021 Nov 3;16(11):e0259535.
[37] Hirsch T, Wahl U. Das praktische Vorgehen beim postoperativen und posttraumatischen Lymphödem [Practical Approaches for Post-Operative and Post-Traumatic Lymphoedemas]. Zentralbl Chir 2017 Jun;142(3):287–96. German.
[38] Pereira de Godoy AC, Ocampos Troitino R, de Fátima Guerreiro Godoy M, Pereira de Godoy JM. Lymph drainage of posttraumatic edema of lower limbs. Case Rep Orthop 2018 Mar 5;2018:7236372.
[39] Thomas C, Le JT, Benson E. Managing lymphedema in fracture care: current concepts and treatment principles. J Am Acad Orthop Surg 2020 Sep 15;28(18):737–41.